ADVANCED HEALTHCARE MATERIALS
www.advhealthmat.de

Engineered Full-Length Fibronectin–Hyaluronic Acid Hydrogels for Stem Cell Engineering

*Sara Trujillo, Sebastián L. Vega, Kwang Hoon Song, Ana San Félix, Matthew J. Dalby, Jason A. Burdick, and Manuel Salmeron-Sanchez**

Mechanical cues induce a variety of downstream effects on cells, including the regulation of stem cell behavior. Cell fate is typically characterized on biomaterial substrates where mechanical and chemical properties can be precisely tuned; however, most of these substrates do not recapitulate the biological complexity of the extracellular matrix (ECM). Here, hydrogels are engineered for mechanobiological studies using two major components of the ECM: hyaluronic acid (HA) and fibronectin (FN). Rather than typical surface chemisorption of FN to substrates, the system contains full-length FN covalently crosslinked to HA throughout the hydrogel. The control over the mechanical properties of the hydrogel independent of the concentration of FN and the ability to culture viable cells either on top or encapsulated within the hydrogels are shown. Interestingly, human mesenchymal stem cells (MSCs) experience an increase in nuclear translocation of the yes-associated protein (YAP) to the nucleus when cultured on (2D) substrates with increasing amounts of FN while maintaining constant hydrogel stiffness. However, this FN dependence on nuclear YAP translocation is not observed for MSCs encapsulated in (3D) hydrogels. This work develops complex hydrogels that recapitulate features of the ECM for the control of stem cells in both 2D and 3D environments.

1. Introduction

Cells respond to a variety of biophysical and biochemical signals within their microenvironment, represented by their extracellular matrix (ECM) when they reside within tissues.[1–4] This may include features such as adhesion to the ECM and the mechanical properties of the surrounding matrix.[5,6] It is now widely understood that cells sense the mechanics of their environment, which has implications in cell signaling and resulting behavior, including control over stem cell differentiation.[3,7] A range of hydrogels have been designed to culture cells atop (2D) or encapsulated within (3D) to probe questions related to mechanobiology. These systems have been intentionally simple to decouple the complexity of the microenvironment; however, there is interest in elevating the complexity to better mimic the synergistic influence of multiple ECM components into our understanding of cellular mechanosensing.

The ECM comprises a range of biochemical components, from proteins to polysaccharides. Common in many tissues (e.g., cartilage) is the polysaccharide hyaluronic acid (HA), a non-sulfated glycosaminoglycan. HA is an important element of the ECM and the structural and biological properties of HA have been implicated in cellular signaling, wound repair, tissue morphogenesis, and matrix organization.[8,9] That is why HA has been extensively used in regenerative medicine.[10] Cells interact with HA through specific cell-surface receptors, CD44 and the receptor for hyaluronan-mediated motility (RHAMM).[11,12] For example, CD44 has an important role in mesenchymal stem cell (MSC) migration[13] and homing.[14,15] HA hydrogels have also been used for in vitro culture and differentiation of embryonic stem cells due to the role of HA in embryogenesis.[16] Furthermore, HA is a major component of cartilage and HA hydrogels have been extensively used to promote chondrogenesis.[17,18]

Recently, HA has become an important building block for the fabrication of new biomaterials used in cell culture and tissue engineering applications.[19] HA can be modified in numerous ways to alter the properties of resulting biomaterials, including their physicochemical features and biological activities. In this sense, HA can be crosslinked into a hydrogel to form a stable scaffold through reaction of various chemical groups such as with aldehydes,[20] divinyl sulfones,[21] or norbornenes.[22]

Dr. S. Trujillo, A. San Félix, Prof. M. J. Dalby, Prof. M. Salmeron-Sanchez
Centre for the Cellular Microenvironment
University of Glasgow
Glasgow G12 8LT, UK
E-mail: Manuel.Salmeron-Sanchez@glasgow.ac.uk
Dr. S. L. Vega
Department of Biomedical Engineering
Rowan University
Glassboro NJ 08028, USA
Dr. K. H. Song
Division of Bioengineering
Incheon National University
Incheon 22012, Korea
Prof. J. A. Burdick
Department of Bioengineering
University of Pennsylvania
Philadelphia PA 19104, USA

The ORCID identification number(s) for the author(s) of this article can be found under https://doi.org/10.1002/adhm.202000989

DOI: 10.1002/adhm.202000989

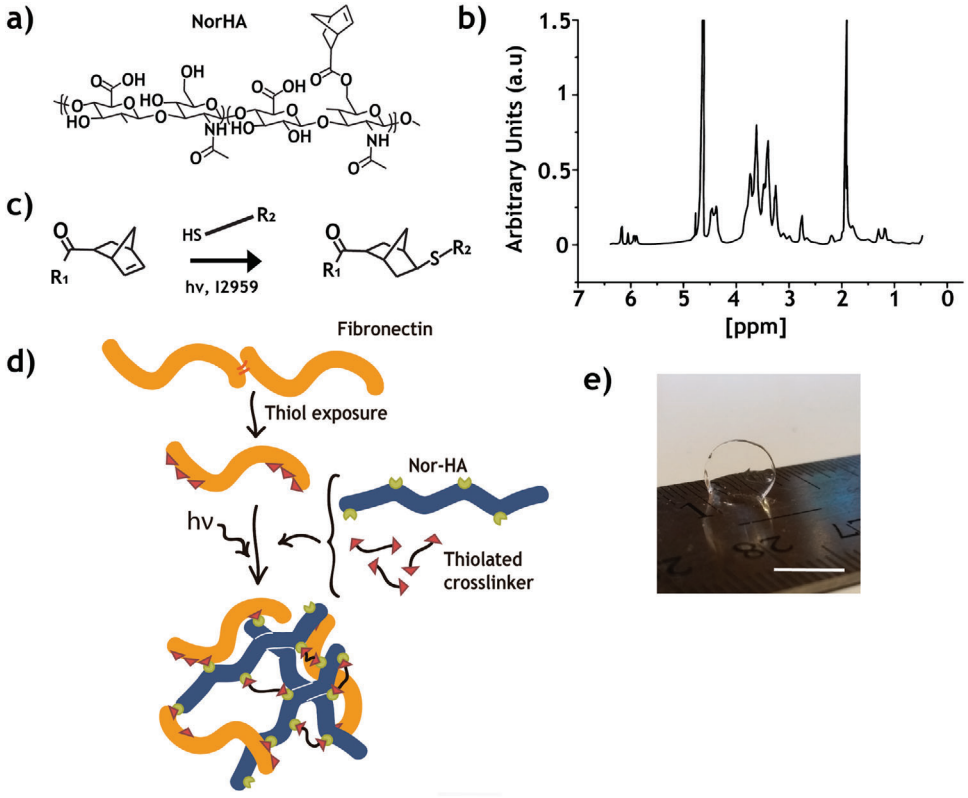

Figure 1. Fabrication of full-length FN–HA hydrogels. a) Chemical structure of NorHA and b) NorHA ^{1}H NMR spectra. c) NorHA reaction with thiols and d) schematic of the formation of hydrogels through the reaction of full-length FN (with exposed thiols) and additional dithiol crosslinker with NorHA. e) Representative image of a FN–HA hydrogel (scale bar: 6 mm).

Norbornenes react through radically induced thiol–norbornene click reactions, which are considered to be highly specific due to the high reactivity of thiols to norbornenes and the low norbornene–norbornene reactivity.[23] Plus, thiol-ene photocrosslinking has been useful to encapsulate molecules and cells while maintaining their bioactivity.[24,25]

Fibronectin (FN) is an abundant glycoprotein that is also found in the ECM, which is classically studied as a cell adhesion protein due to its Arg-Gly-Asp (RGD) and Pro-His-Ser-Arg-Asp (PHSRN) motifs.[26–28] FN or its peptides have been critically used to functionalize materials in mechanotransduction and cell differentiation studies. FN is commonly adsorbed onto different surfaces such as polyacrylamide and poly(ethylene glycol) (PEG).[29–32] Depending on the surface properties, FN adsorption leads to different protein conformations, which can enhance adhesion[33] or change FN conformation to reveal cryptic sites,[34] such as the heparin-binding site that has been shown to promiscuously bind growth factors.[35–38] Apart from its RGD motif and affinity to several growth factors, FN can bind several other molecules such as other FN molecules (which support fibrillogenesis),[39,40] collagen,[41] fibrin, or proteoglycans (e.g., syndecans).[42] Moreover, FN also contains non-RGD-binding integrin motifs.[43] Altogether, this shows the biological importance of FN and its versatility for use in biomedical applications.

To introduce some complexity of the ECM, we fabricated hydrogels from both HA and FN. Specifically, we demonstrate that full-length FN can be covalently crosslinked into an HA hydrogel using thiol-ene photocrosslinking to engineer FN–HA hydrogels with controlled mechanical properties. We show that key properties, such as the accessibility of the adhesion motif, of the FN molecule are maintained after incorporation into hydrogels. This work introduces a new family of hydrogels that recapitulate properties of the ECM by incorporating full proteins, without small peptides, or other synthetic components,[44,45] as a platform for 2D and 3D mechanobiological studies.

2. Results and Discussion

2.1. FN–HA Hydrogels via Thiol-Ene Reaction

We used thiol-ene chemistry to fabricate a hydrogel that incorporates components of the ECM.[22] We first modified HA with functional groups to permit crosslinking into hydrogels. Specifically, HA was modified with norbornene groups following previous protocols to form norbornene-modified HA (NorHA) (**Figure 1**a).[4,22] The synthesized NorHA consisted of ≈20% of its repeating units functionalized with norbornene groups, as analyzed by nuclear magnetic resonance (^{1}H NMR) (Figure 1b). Peaks at 6.3–6.2 correspond to vinyl protons, directly attached to the C=C double bond of the norbornene ring, peaks at 3.0–2.8 and at 1.8–1.0 correspond to the bridge and ring protons.[22,46]

Norbornenes react with thiolated compounds via light-mediated thiol-ene addition reactions in the presence of a photoinitiator, such as I2959 and UV light (Figure 1c). This strat-

egy allows control over hydrogel mechanics, which is controlled by tuning crosslinking density.[22] To form hydrogels that also include the ECM component FN, we leveraged the cysteine residues (that carry a thiol group in the side-chain) naturally present on FN, which can be exposed via protein chemical unfolding (Figure 1d).[22] Chemical unfolding was achieved using tris(2-carboxyethyl)phosphine hydrochloride (TCEP), which has been previously used to expose thiol groups to PEGylate FN and other proteins such as fibrinogen.[44,45]

FN has been previously incorporated into HA hydrogels using PEG functionalized with *N*-hydroxysuccinimide ester as a crosslinker agent that targets the free amino groups on FN.[47] This approach increases the probability of blocking key FN binding sites since amino groups are randomly distributed throughout the molecule. In our case, we linked FN directly to the HA backbone by exposing thiol groups that are located at the ends of the FN molecule. This results in a targeted protein crosslinking approach and, we have previously shown that this type of modification (using TCEP) does not affect critical FN binding sites including cell adhesion and growth factor binding domains.[44]

Further, we also used two different thiolated crosslinkers: either dithiothreitol (DTT) or a protease-degradable peptide (GCRDVPMSMRGGDRCG). This approach has been used before to fabricate nondegradable or degradable HA hydrogels, respectively.[4,48] Cell-mediated degradation (e.g., using a protease-sensitive peptide as a crosslinker) allows cells to spread and migrate within the hydrogel, and previous HA hydrogel systems that incorporate FN lack this critical feature for 3D cell culture.[4,47,49,50] Thus, our design resulted in the fabrication of optically transparent (Figure 1e) FN–HA hydrogels with controllable crosslinking density and degradation.

2.2. FN Incorporation into HA Hydrogels

To assess the incorporation of FN within the hydrogels, we fabricated HA hydrogels using either chemically unfolded FN (i.e., using TCEP to expose thiol groups) or native FN (i.e., without exposing thiol groups). Hydrogels are labeled HA XFN, where X is the concentration of FN incorporated into the hydrogel in micrograms per milliliter. After forming the hydrogels, we performed a series of washes to remove any uncrosslinked protein from the hydrogel before visualizing remaining FN with immunostaining (**Figure 2**a–d). FN was detected in all FN–HA hydrogels, both when nondegradable using DTT as a crosslinker (Figure 2a) or degradable using a protease-degradable peptide (Figure 2b), confirming the incorporation of FN into HA hydrogels. Moreover, FN was detected homogeneously when imaging both from the hydrogel surface or cross section.

As expected, FN was not detected in the controls of HA-only hydrogels where FN was not included during formation (Figure 2c). Additionally, FN was not visualized in the hydrogels fabricated with only native FN (Figure 2d), meaning that FN diffused from hydrogels without covalent crosslinking. This emphasizes the importance of the crosslinking strategy outlined in Figure 1 to retain the FN within the hydrogel.

To further explore the efficiency of crosslinking using thiol-ene chemistry, we performed a FN release study where we tracked the diffusion of FN from the hydrogels. We fluorescently tagged FN that was incorporated into NorHA hydrogels with either thiols exposed (to covalently bind the protein) or in its native form (to physically trap the protein). As seen in Figure 2e, when FN is not crosslinked (i.e., just physically trapped into the HA network), there is constant release of FN for 7 days (i.e., FN is diffusing from the hydrogel as it is not crosslinked), whereas when FN is crosslinked to NorHA, there is a first burst release (although 30% lower than the burst release for the uncrosslinked counterpart) and afterwards FN release drops continuously, until being undetectable after 4 days, demonstrating the stability of the covalent binding of FN into the NorHA network.

2.3. Mechanical Properties of FN–HA Hydrogels Can Be Controlled

The mechanical properties of the hydrogels were tested in compression using dynamic mechanical analysis (DMA). As shown in Figure 2f, the elastic modulus increased monotonically with increasing crosslinker concentration up to an X_{DTT} (ratio between thiol and norbornene groups) of 1. When surpassing an equal number of norbornene groups and thiol groups, the modulus starts to decrease. The excess in thiol groups means that not all crosslinkers are fully reacted and form effective crosslinks as has been previously discussed on similar hydrogel systems that use thiol-ene chemistry.[22,51,52] The range of moduli observed was from <1 to 15 kPa, for the concentration of NorHA used (2 wt%). This range could be further tuned by using different NorHA concentrations or HA with higher norbornene modifications.[22]

We selected a crosslinker concentration of X_{DTT} equal to 0.6, which presented an elastic modulus of ≈7 kPa (Figure 2f). This range was chosen to be able to study early cell adhesion, focal adhesion (FA) formation, and nuclear YAP translocation.[31] We also selected this crosslinker density to fabricate FN–HA hydrogels that retained enough norbornenes for incorporation of increasing amounts of FN (up to 2000 μg mL^{-1} compared to tenfold lower FN incorporation in HA hydrogels by others[47,49]).

Then, the mechanical properties of these hydrogels with increasing amounts of FN were characterized (Figure 2g). Interestingly, all hydrogels had similar average elastic moduli of ≈7 kPa (no statistically significant differences), independent of the final concentration of FN used. This implies that although various FN amounts can be incorporated into hydrogels, the mechanics are largely driven by the initial crosslinker amount (X_{DTT}). A similar observation was described recently for synthetic PEG hydrogels with and without FN.[44] In this case, the concentration of FN did not alter the elastic modulus measured by nanoindentation. We expect, however, to see an effect in the viscosity of the hydrogels with increasing amounts of FN added, as we only tested the bulk elastic modulus of the hydrogels. This further demonstrates that we can engineer hydrogels with different amounts of FN incorporated while maintaining the same mechanical properties, which is particularly interesting to allow probing of the influence of the microenvironment on cell behavior.

2.4. MSCs on FN–HA Hydrogels

Human MSCs were seeded on FN–HA hydrogels containing different amounts of FN (**Figure 3**). MSCs on hydrogels without FN

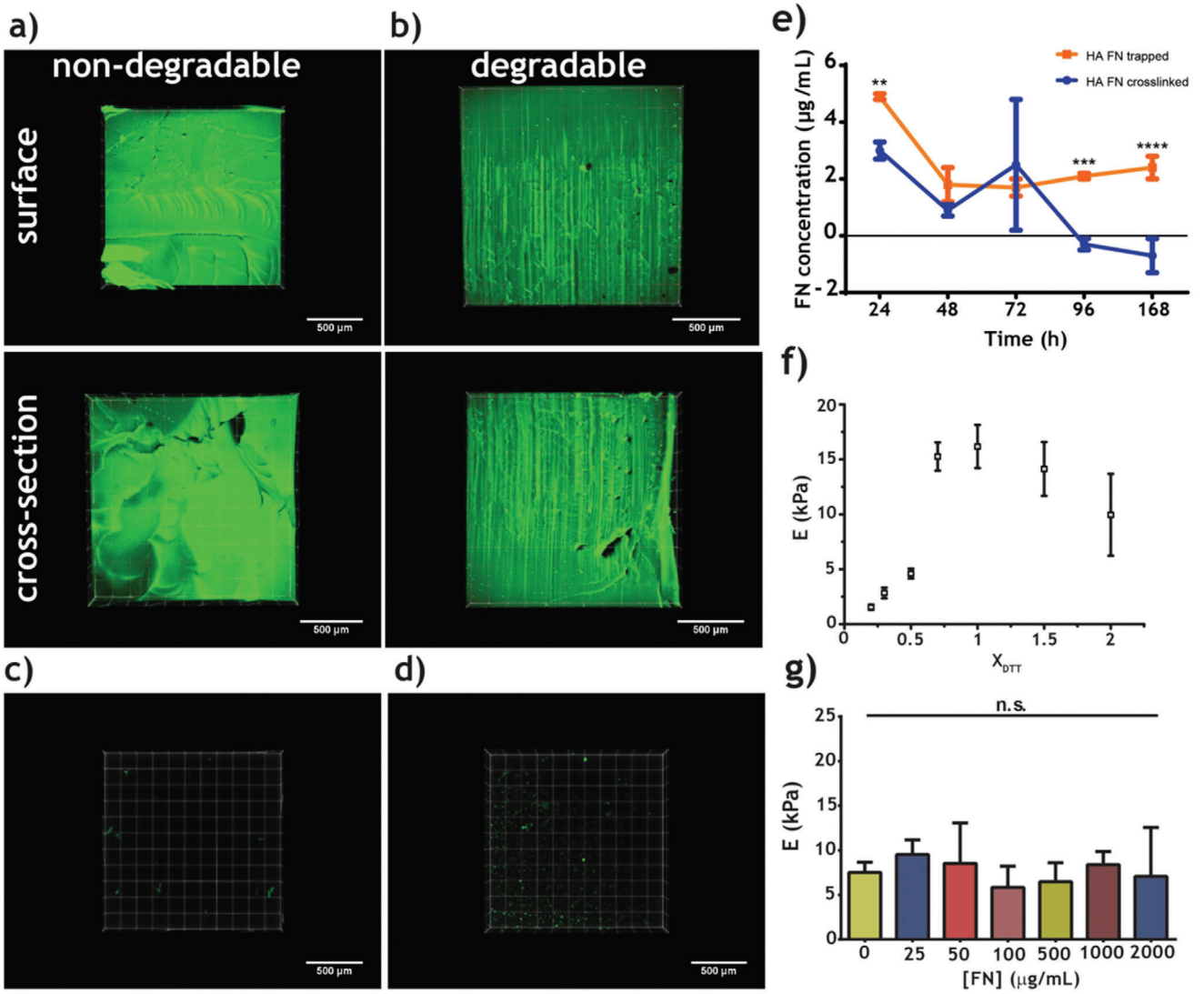

Figure 2. FN incorporated into HA hydrogels with controlled mechanical properties. a) Nondegradable (DTT crosslinker) and b) degradable (protease-degradable peptide crosslinker) HA 50FN hydrogel surface (top) and cross section (bottom). c) HA 0FN and d) HA with native (not unfolded) FN. Scale bar: 500 µm. e) FN release from either hydrogels with FN crosslinked (blue) or physically trapped (non-crosslinked, orange) (mean ± SD, $n = 3$, measured in triplicate); $^{**}p < 0.01$, $^{***}p < 0.005$, $^{****}p < 0.001$ via t-test for each time point. f) Elastic modulus of HA 0FN hydrogels using different crosslinking densities (X_{DTT} is the ratio between thiol from DTT to norbornene from NorHA). g) Elastic modulus of FN–HA hydrogels using different concentrations of FN (X_{DTT} 0.6). Graphs show mean ± SD ($n = 3$, measured twice); n.s, not statistically different via ANOVA.

(HA 0FN) showed minimal spreading, with diffuse actin staining and a rounded morphology (Figure 3a). MSCs spread well and developed well-defined actin stress fibers on FN–HA hydrogels but no change in cell spreading was noted with increasing amounts of FN incorporation, from 50 µg mL^{-1} FN up to 500 µg mL^{-1} (HA 50FN and HA 500FN, Figure 3a–d). This suggests that the amount of adhesion domains available on the surface of the material was already saturated at 50 µg mL^{-1} of FN and, as the mechanical properties of the hydrogels are similar (≈7 kPa), cells did not reflect any differences in morphology as quantified by cell shape descriptors (i.e., total cell area, aspect ratio, roundness) (Figure 3b–d). To further investigate this, we performed a vinculin staining to look at FA formation at early stages to see whether increasing amounts of FN would result in larger FAs (3 h) (Figure 3e–h). Interestingly, we only detected FAs in cells seeded on HA 500FN, as can be seen by the number of FAs quantified (Figure 3f), whereas vinculin staining was diffused and mainly cytoplasmic in cells seeded on HA 50FN, even when cells spread similarly on both HA 50FN and HA 500FN. The quantification of both HA 0FN and HA 50FN suggests no FA formation (Figure 3f–h) as cells still adhere and spread onto the surface of HA 50FN hydrogels. This finding suggests the importance of the role of HA in the initial cell adhesion, providing early cell attachment on both HA 0FN and HA 50FN that is not integrin related. As expected, FA formation does not occur in cells seeded on HA 0FN as HA has no receptors for integrins.

In order to study the role of HA in MSC attachment, we performed early adhesion studies (3 h) to look at the cell-surface

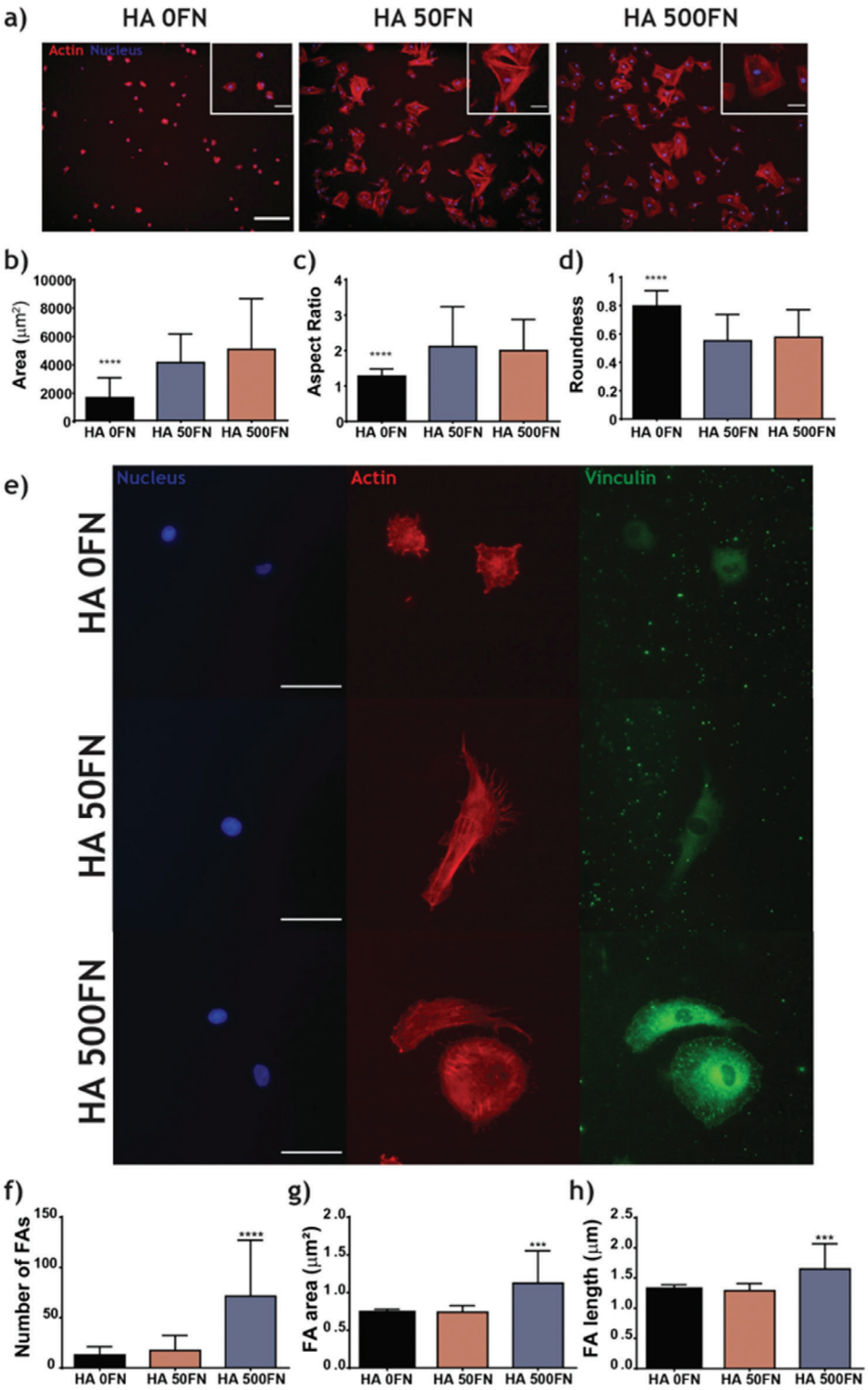

Figure 3. MSCs attach and spread onto FN–HA hydrogels. MSCs seeded on top of FNHA hydrogels with different amounts of FN (depicted as XFN where X is the total amount of FN in micrograms per milliliter) for 3 h and assessed for spreading via a) imaging after staining for actin and nuclei (scale bar: 200 μm, inset scale bar: 50 μm). Quantification of cell spreading was performed by measuring cell b) spread area (μm^2), c) aspect ratio, and d) roundness (mean ±SD, $n > 100$ cells, conditions in triplicate). Statistical differences determined with Kruskal–Wallis test followed by Dunn's post hoc test to correct for multiple comparisons where $^{****}p < 0.0001$. e) Representative images of FA formation after 3 h, nuclei (blue), actin (red), and vinculin (green) (scale bar: 50 μm). Graphs (mean ± SD, $n > 10$ cells) showing the f) FA analysis with the number of FA per cell, g) the average FA area per cell (μm^2), and h) the average FA length per cell (μm).

receptor CD44, which is one of the main proteins used by cells to bind HA (**Figure 4**).[53,54] Cells seeded on top of HA 0FN hydrogels presented high signal for CD44 and form clusters (Figure 4a). Cells seeded on HA 50FN and HA 500FN also presented CD44 staining, with less cluster formation and a more diffused staining throughout the cytoplasm. This suggests that cells on HA 0FN reorganize CD44. On hydrogels with FN, it is reasonable to think that both CD44 and integrin binding are occurring at the same time and so there could be less reorganization due to competition between these two modes of attachment. On the other hand, when MSCs were blocked for CD44 prior to seeding (Figure 4b), we observed little to no attachment on HA 0FN hydrogels, with the few cells that remained on the gels presenting a rounded morphology and a smaller cell area (Figure 4d). Differences were observed when comparing cell areas with and without blocked CD44 (Figure 4c,d). On HA hydrogels without FN, cells could not attach as shown by a dramatic drop in cell area measurements. When comparing hydrogels with FN, cells were able to attach and spread, but the overall cell areas decreased when CD44 was blocked. More interestingly, cell areas decrease more on HA 50FN compared to HA 500FN when CD44 is blocked. This provides additional support to the role that HA has on early MSC attachment. We also quantified CD44 cluster formation as if they were FAs (Figure S1, Supporting Information; Figure 4e). We found that cells seeded on HA 0FN developed bigger CD44 clusters compared to FN–HA hydrogels (as measured by cluster area, Figure S1a, Supporting Information) and these differences are even more noticeable when the areas of the CD44 clusters are normalized by cell size (Figure 4e). This normalization is important because cells on top of HA 0FN hydrogels are significantly smaller compared to hydrogels with FN.

Yes-associated protein (YAP) has emerged as an important marker of a cell response to local mechanical properties, acting as a mechanical rheostat. YAP/TAZ are considered master regulators of mechanotransduction, being of critical importance in translating external mechanical signals (e.g., ECM stiffness) to the nucleus and initiating downstream signaling through the Hippo pathway.[55] Nuclear translocation of YAP has been shown to depend not only on the stiffness of the material but also on other parameters such as dimensionality and degradability.[4] **Figure 5**a shows the translocation of YAP for MSCs seeded on top of HA FN hydrogels. For HA 0FN hydrogels (no FN)-only diffuse, YAP staining was present in MSCs and mainly localized in the cytoplasm, whereas cells seeded on top of hydrogels containing FN (i.e., HA 50FN and HA 500FN hydrogels) presented YAP staining in both the cytoplasm and, more notably, nucleus. These events were further confirmed after quantification of the YAP nuclear to cytoplasm ($YAP_{nuc/cyt}$) ratio (Figure 5b), where a trend was observed with the localization of YAP, correlating to increasing amounts of FN in hydrogels, even though the elastic modulus was similar across all formulations (X_{DTT} 0.6, ≈7 kPa). Classically, 2D substrates present a correlation between elevated substrate stiffness and nuclear translocation of YAP,[55] where cell spreading can regulate YAP/TAZ translocation to the nucleus independent of the available adhesion area.[55]

Our data suggest that the amount of FN incorporated into HA FN hydrogels plays a role in the nuclear translocation of YAP. For example, Elosegui-Artola et al. reported that cell traction forces decreased when cells were seeded on top of the substrates with lower FN density (100 μg mL^{-1}).[56] Cell traction forces are also dependent on RGD spacing on hydrogels.[57] Thus, it may be expected that FN concentration would impact YAP in our system.

More fundamental studies have been performed using RGD peptide tethering to investigate the relationship between ligand density and cell behavior. Cell adhesion generally shows a sigmoidal increase as a function of RGD concentration.[58] This means that there is a critical minimum ligand density for cell response. Massia and Hubbell found that cells need a minimum of 1 fmol of RGD cm^{-2} for spreading and 10 fmol RGD cm^{-2} to form FAs and stress fibers.[59] Similar results have been shown by Rowley and Mooney using alginate-RGD gels.[60] Taken together, the FN density readily available on the surface of the FN–HA hydrogels could be an important asset for 2D adhesion studies. Considering a hydrogel containing 50 μg mL^{-1} of FN (HA 50FN) and considering also a homogeneous and isotropic distribution of the protein through the first 10 nm of the hydrogel, the superficial density of RGD of the hydrogel would be ≈200 fmol cm^{-2}. This is 20-fold more theoretical RGD compared to the minimum needed to form FAs.[59] However, there are no FA formations on these hydrogels but there are actin stress fibers. This suggests that HA is also playing a critical role in early cell attachment and that CD44 molecules interfere in the organization of FAs.

This hydrogel system could be used not only to study the effect of FN concentration in 2D and 3D, but also, due to the presence of full-length FN, we anticipate that the system could be loaded with growth factors, which can bind to the heparin II binding domain on FN,[35] and thus be an invaluable platform to unveil the relationship between growth factor signaling and mechanotransduction in stem cell engineering.

2.5. MSCs in 3D FN–HA Hydrogels

After the initial characterization of this new hydrogel system, we tested whether MSCs survive encapsulation. **Figure 6**a shows the results for a Live/Dead staining at 3 days. MSC viability (Figure 6b) was equal or greater than 80%, which shows high cytocompatibility. As expected, this result confirms previous literature on the suitability of ultraviolet light-triggered thiol-ene reactions for 3D cell culture as well as when FN is crosslinked.[4,22,61] We also studied cell spreading and YAP translocation in 3D after 7 days (Figure 6c–f). Cell areas were bigger in cells seeded within FN–HA hydrogels even though the aspect ratio was similar in conditions with and without FN (Figure 6c,d). This shows that cells are able to spread also in 3D using this system. No differences in cell area were found between HA 50FN and HA 500FN. In addition, we looked at YAP translocation to the nucleus in 3D (Figure 6e,f) and we did not find significant differences in the signal of YAP between nucleus and cytoplasm, contrary to what we found in 2D culture, where we detected an increase of YAP translocation to the nucleus with increasing amounts of FN. YAP nuclear translocation in HA hydrogels was previously reported to be affected by dimensionality and, more specifically, by cell spreading in 3D compared to 2D.[4] This could explain why we observe similar levels of YAP nuclear translocation, as cell spreading is similar among the three conditions tested (defined by the aspect ratio) even when the average cell areas are bigger in FN–HA hydrogels compared to HA only hydrogels. In this case, all

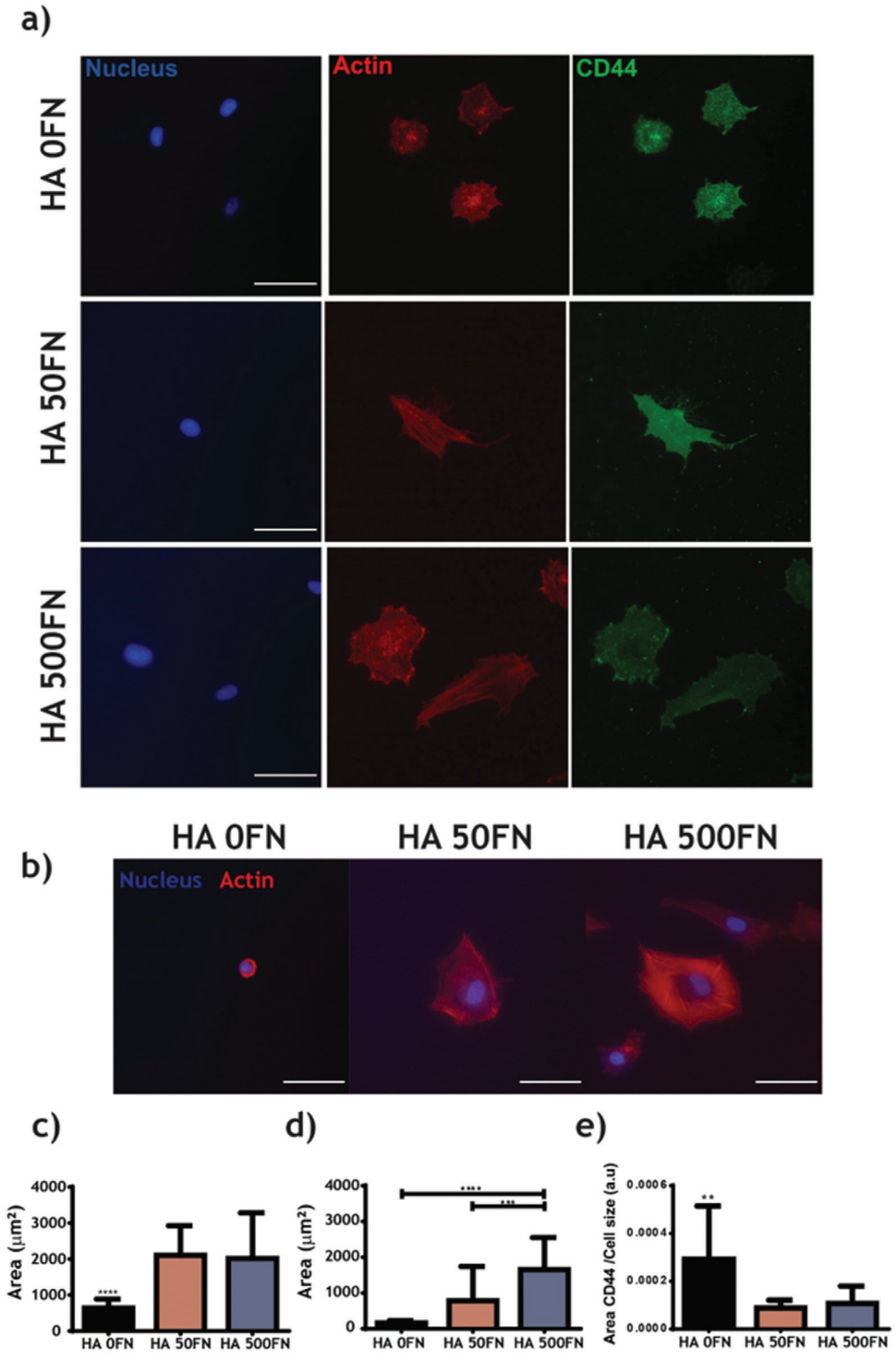

Figure 4. Effect of HA in MSC attachment and spreading via CD44. MSCs were seeded on top of HA 0FN, HA 50FN, and HA 500FN hydrogels with and without CD44 blocked, to study the effect of HA on cell attachment after 3 h. a) Representative images of cells where the nucleus is depicted in blue, the actin cytoskeleton in red, and CD44 in green (scale bar: 50 μm). b) Representative images of MSCs with CD44 blocked prior to seeding on HA 0FN, HA 50FN, and HA 500FN hydrogels for 3 h, nuclei (blue), actin (red) (scale bar: 50 μm). c) Cell areas for MSC adhesion after 3 h without blocking CD44 and d) cell areas for MSCs with CD44 blocked prior seeding on hydrogels for 3 h. (mean ± SD, $n > 15$ cells, except for HA 0FN with CD44 blocked as there were not enough cells attached). ****$p < 0.001$, ***$p < 0.005$.

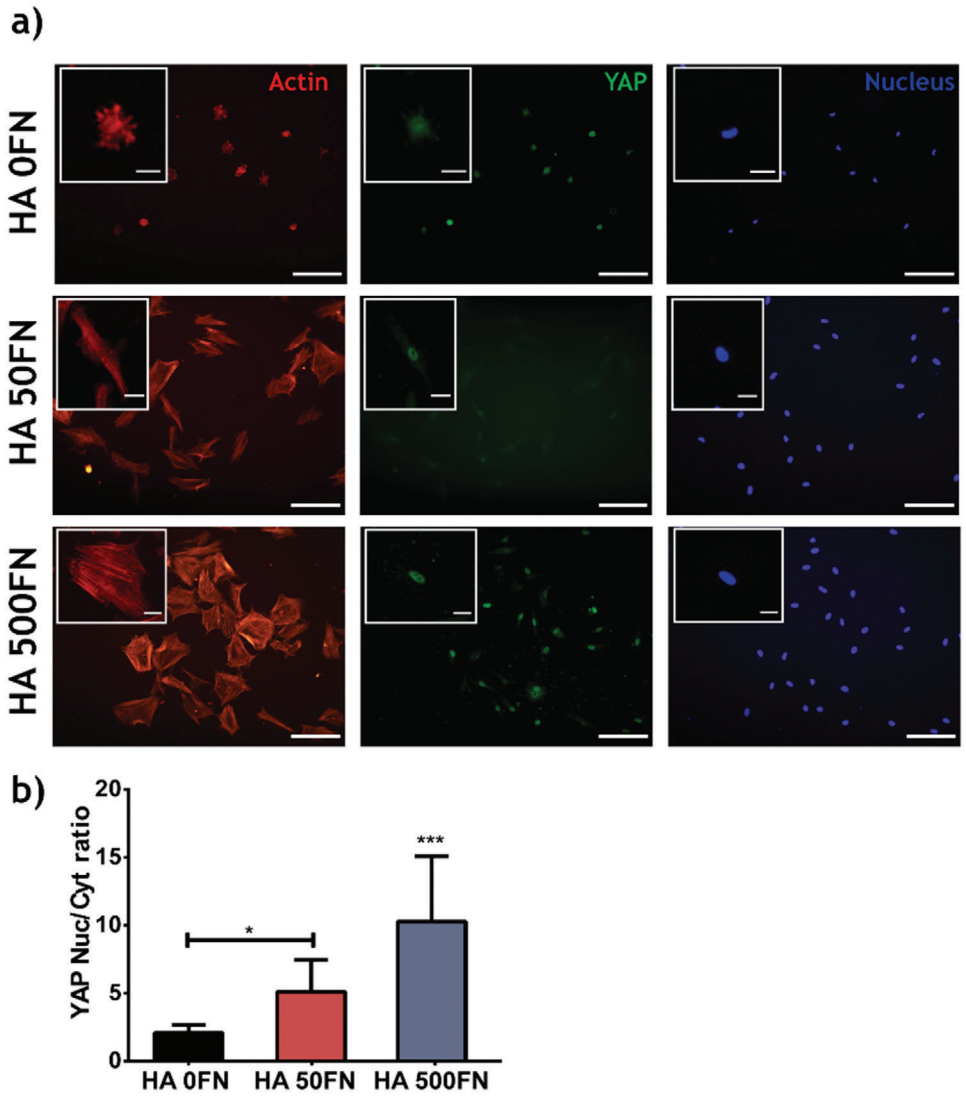

Figure 5. Increased translocation of YAP into the nucleus with increasing amounts of FN on the same hydrogel stiffness (≈7 kPa, X_{DTT} 0.6). MSCs seeded on FN–HA hydrogels with different amounts of FN (depicted as XFN where X is the total amount of FN in micrograms per milliliter) for 3 h. a) Representative images of cells (scale bar: 200 µm, inset: 50 µm), where red depicts actin, green YAP, and blue nuclei, respectively. b) YAP nuc/cyt ratio as a function of the amount of FN used within the gels (0, 25, 50, or 500 µg mL^{-1}). Data shown as mean ± SD ($n \geq 15$ cells, conditions in triplicate) with significant differences determined with ANOVA followed by Tukey's post hoc test where $^{*}p < 0.5$ and $^{***}p < 0.005$.

hydrogels were degradable, as they were crosslinked using the protease-sensitive peptide. Future studies are needed to understand the effects of both increasing degradability and increasing amounts of FN in hydrogels of similar stiffness on YAP nuclear translocation.

FN has been previously grafted onto a HA hydrogel for the 3D culture of endothelial cells.[47,49] Photocrosslinnking via acrylate groups was used to incorporate a previously PEGylated FN. FN was incorporated up to 500 µg mL^{-1}, whereas we prepared hydrogels with increasing amounts of FN and up to 2 mg mL^{-1}. Furthermore, they showed that the viability of endothelial cells was around 40–50% except for the conditions with more FN incorporated that reached 90% viability. In our case, the viability of HA 0FN (no FN) was as high as conditions with FN, showing that the methodology of encapsulation is highly cytocompatible and robust.[17] In summary, MSC viability after encapsulation via thiol-ene UV-initiated photocrosslinking shows that this system allows the in situ encapsulation of cells and cell spreading, proving its suitability as a 3D microenvironment too.[25]

3. Conclusions

We show a new approach to incorporate full-length FN into a natural HA hydrogel by synthesizing a norbornene-functionalized HA and using it to directly and covalently bind FN during UV-triggered thiol-ene crosslinking. These hydrogels were fabricated to incorporate different amounts of FN. The mechanical properties were controlled independently of the amount of FN tethered and MSCs respond to both HA and FN via CD44 and integrin binding respectively. These hydrogels also supported 3D encap-

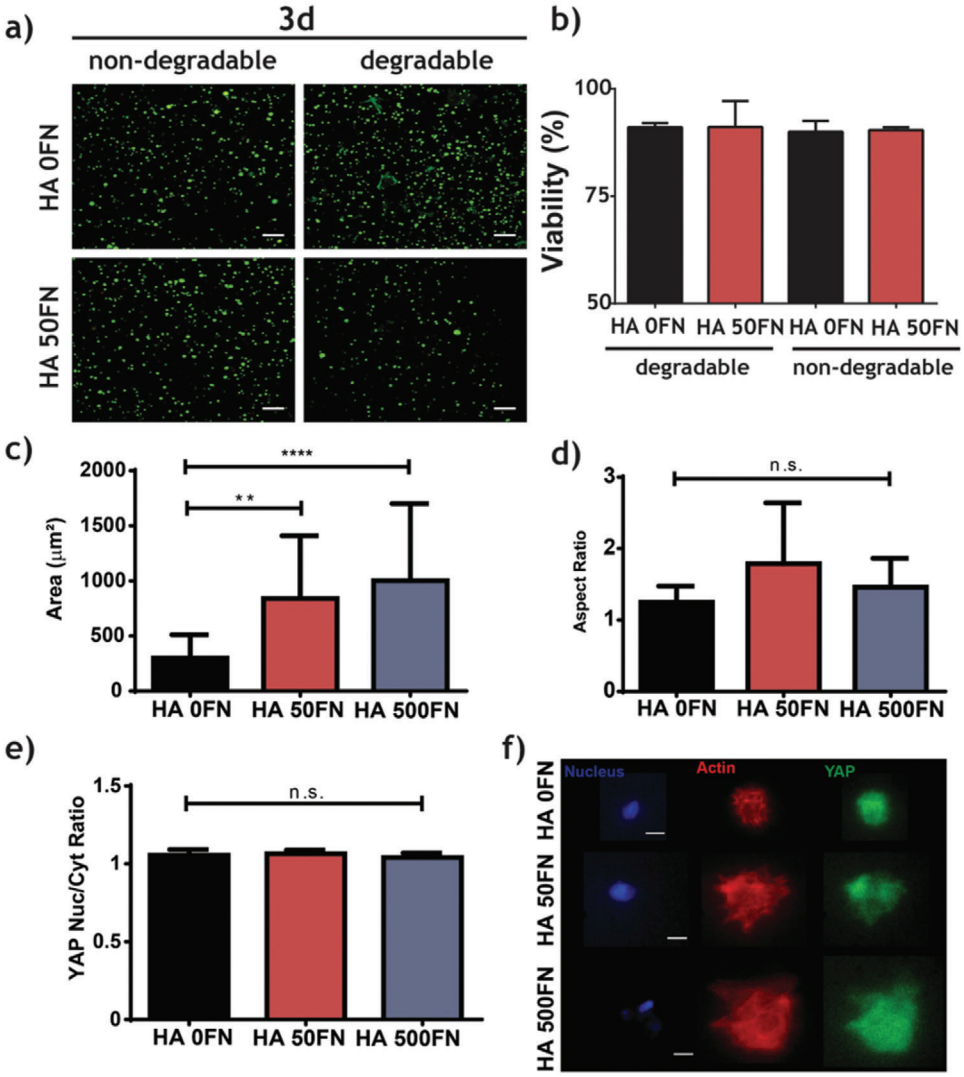

Figure 6. MSCs encapsulated within FN–HA hydrogels show high viability. MSCs were encapsulated within FN–HA hydrogels incorporating either nondegradable or degradable hydrogels and without and with FN (0FN and 50FN, 0 and 50 mg mL^{-1}, respectively) for 3 days and their viability was assessed by Live/Dead staining. a) Maximum *Z*-axis projection of a stack of images from the Live/Dead staining of different FN–HA hydrogels where green and red represent live and red dead cells, respectively, for 3 days of culture (scale bar: 200 mm) and b) quantification of viability (mean ± SD, $n = 3$, samples in triplicate) after 3 days of culture. c) Area (μm^2) and d) aspect ratio of cells after 7 days in culture (mean ± SD, $n > 10$ cells). e) Quantification of YAP nuclear translocation in 3D after 7 days of culture (mean ± SD, $n > 10$). f) Representative images of nucleus (blue), actin (red), and YAP (green) staining (scale bar: 10 μm).

sulation and spreading of MSCs. This material is versatile system that could be used as a platform for fundamental studies for stem cell engineering, both in 2D and 3D.

4. Experimental Section

NorHA Synthesis: HA was first modified using tetrabutylammonium salt (HA-TBA). Briefly, sodium hyaluronate (Na-HA, Lifecore Biomedical, ≈75 kDa) was dissolved in deionized (DI) water at a concentration of 20 mg mL^{-1}. Once dissolved, Dowex resin (50WX8, Sigma) was added to the solution at a resin to Na-HA ratio of 3:1 w/w for 2 h while stirring at room temperature. Then, the mixture HA/resin was filtered using a Kitasato flask (Whatman paper #2, vacuum). After that, a solution of TBA in DI water was prepared (1:1 v/v). Neutralization of the HA solution was performed using TBA solution, until pH 7.02–7.05. Once neutral, the solution was partitioned into 50 mL tubes, frozen (–80 °C, overnight), and lyophilized (4 days, <130E-03 mBar, –80 °C). The product of lyophilization was stored at –20 °C until use. ^{1}H NMR spectrum of HA-TBA was performed dissolving 5 mg of HA-TBA in 700 μL of D_2O; the spectrum obtained was used to confirm the degree of modification.

NorHA was synthesized by mixing HA-TBA with 5-norbornene-2-methylamine (Nor-amine) and anhydrous dimethyl sulfoxide (DMSO, Sigma) (≈5 mL per 0.1 g HA-TBA, via cannulation) in a round bottom flask under inert atmosphere. Once HA was fully dissolved, a benzotriazole-1-yl-oxy-tris-(dimethylamino)-phosphonium hexafluorophosphate

Table 1. HA hydrogels formulations used. SH groups coming from the crosslinker, either DTT (nondegradable) or protease-degradable peptide (GCRDVPMSMRGGDRCG, degradable) were used.

HA hydrogels	HA XFN
NorHA [mg mL^{-1}]	20
FN [μg mL^{-1}]	X (0; 25; 50; 100; 500; 1000; 2000)
Ratio SH/Nor	0.6:1 (unless otherwise noticed)

(BOP, in DMSO) solution was added via cannulation to the HA/Nor-amine solution and it was reacted for 2 h at room temperature. After reaction, the solution was quenched with cold DI water and transferred to a presoaked dialysis tube (MWCO 6–8 kDa). Dialysis was performed for 5 days in DI water (adding 5 g NaCl in the dialysis water, changing water twice daily). Then, the dialyzed product was filtered using a Kitasato flask (Whatman paper #2, vacuum). The filtered product was dialyzed again in DI water for 3–5 days. The dialyzed product was partitioned into 50 mL tubes, frozen overnight, and lyophilized for 4 days. ^{1}H NMR spectrum of NorHA was performed dissolving 5 mg of Nor-HA in 700 μL of D_2O; the spectrum obtained was used to confirm the degree of modification.

HA Hydrogel Polymerization: Solutions containing NorHA (2 wt%), DTT (Sigma), Irgacure 2959 (2-hydroxy-4′-(2-hydroxyethoxy)-2-methylpropiophenone, Sigma, 0.05 wt%), and Dulbecco's phosphate-buffered saline (DPBS, Gibco) were prepared using different formulations (**Table 1**). Once dissolved, 70 μL of the solution was placed on a polydimethylsiloxane (PDMS) mold and the samples were covered with a glass coverslip. Then, samples were photopolymerized (Excelitas Omnicure S1500, filter 320–390 nm, 10 min, 10 mW cm^{-2}).

For FN–HA hydrogels, FN was denatured using 20×10^{-3} M tris(2-carboxyethyl)phosphine hydrochloride (TCEP) for 15 min. Then, the denatured FN was mixed with the HA solution for 10 min and hydrogels were formed by photopolymerization (10 min, 10 mW cm^{-2}) using DTT or an in-house synthesized protease-degradable peptide (GCRDVPMSMRGGDRCG) as crosslinkers.

For cell encapsulation experiments, cells were resuspended in HA polymer solution at a final density of 10^6 cells mL^{-1}. The solution with cells was added to a 6 mm cylindrical mold and irradiated for 10 min at 10 mW cm^{-2}. The newly formed gels were immediately transferred to a 24-well plate with a growth medium.

DMA Tests: Mechanical tests were performed using a DMA Q800 (TA Instruments) in compression mode. F a force ramp of 0.5 N min^{-1} was applied up to 15 N of force were reached. The compressive modulus (E) was obtained from stress–strain curves and calculated as the slope between 10% and 20% strain using TA Instruments software. Conditions were prepared in triplicate. Each sample was measured twice.

Cell Adhesion Assay on NorHA Hydrogels: For cell adhesion experiments, human primary MSCs (from bone marrow, PromoCell) were grown in 10 mm petri dishes using growth medium (*α-Modified Eagle's Medium (α*-MEM) and 10% fetal bovine serum (FBS, Gibco)). All hydrogels were polymerized and maintained in DPBS until seeding. Cells were seeded on top of the hydrogels at a density of 5000 cells cm^{-2} for 3 h in medium without serum. Glass controls were seeded at the same cell density using growth medium. Cells were fixed using 4% paraformaldehyde for 30 min at room temperature. Samples were washed twice with DPBS after fixation and kept at 4 °C until immunostaining was performed.

CD44-blocking experiments were performed incubating MSCs with mouse-anti-CD44 (dilution 3:1000 in 2% FBS/DPBS v/v buffer)[53,62] for 45 min on ice. Cells were washed twice in 2% FBS/DPBS and resuspended in growth media without serum for seeding.

Cell Viability: Cytocompatibility of hydrogels with MSCs was tested using Live/Dead assay (Thermo Fisher) following manufacturer's instructions. Briefly, samples were washed twice in DPBS and then immersed in 2×10^{-3} M calcein-AM and 4×10^{-3} M ethidium homodimer-1 and incubated for 15 min. Then, samples were washed twice with DPBS and imaged using a confocal microscope (Leica) at 10× and 20× magnification.

Immunostaining: FN was detected via immunostaining in hydrogel samples. Hydrogels were blocked with blocking buffer (1% bovine seroalbumin (BSA) in DPBS) for 30 min at room temperature. Then, primary antibody rabbit polyclonal-anti-FN (Sigma) was added and incubated for 1 h at room temperature. After the addition of the primary antibody, samples were washed three times using washing buffer (0.5% Tween 20 in DPBS). Then, secondary antibody goat-anti-rabbit-Cy3 was incubated for 1 h at room temperature (protected from light). After that, samples were washed three times using washing buffer. Images were taken using a confocal microscope (Leica).

Immunostaining to detect YAP was performed as follows. First, cells were permeabilized with 0.1% Triton X-100 (Sigma) for 5 min and blocked with 3% BSA for 45 min. After blocking, the primary antibody rabbit-anti-YAP was added and incubated overnight at 4 °C (Santa Cruz Biotechnology, dilution 1:200). Then, the primary antibody was washed thrice with washing buffer. After washing, a secondary antibody goat-anti-rabbit-Alexa Fluor 488 was added for 2 h at room temperature (Thermo Fisher, dilution 1:200). Three washes with washing buffer follow the antibody incubation. Then, rhodamine phalloidin was added for 20 min (Thermo Fisher, dilution 1:200) and 4′,6-diamidino-2-fenilindol (Thermo Fisher, DAPI) staining for 10 min (dilution 1:5000). Images were taken using an epifluorescence microscope (Nikon) at 20× magnification. For 3D experiments, hydrogels were mounted using VECTASHIELD (Vector Laboratories) mounting medium on bottom glass petri dishes and images were taken using an epifluorescence microscope (ZEISS) at 20× and 40× magnification.

Immunostaining to detect vinculin/CD44 was performed as follows. First, cells were permeabilized with 0.1% Triton X-100 (Sigma) for 5 min and blocked with 1% BSA for 30 min. After blocking, the primary antibody mouse-anti-vinculin (Sigma, dilution 1:400)/mouse-anti-CD44 (Abcam, dilution 1:200) was added and incubated for 1 h at room temperature. Then, the primary antibody was washed thrice with washing buffer. After washing, a secondary antibody rabbit-anti-mouse-Cy3 was added for 1 h at room temperature (Jackson ImmunoResearch, dilution 1:200) together with 488-phalloidin (Thermo Fisher, dilution 1:200). Then, samples were washed five times with washing buffer and mounted using VECTASHIELD with DAPI (Vector Laboratories).

Image Analysis—Cell Morphology Analysis: Cell shape descriptors were measured using ImageJ 1.51v (National Institutes of Health, USA). Briefly, actin cytoskeleton images were binarized using a threshold function. Then, the wand tracing tool was used to select the outline of the cell and the measure function was used to calculate parameters such as cell area, aspect ratio, and roundness. The aspect ratio is defined as the ratio between the major and minor axis of the shape selected and the roundness was calculated as follows:

Equation (1): Roundness calculation

$$\text{Roundness} = (4 \times \text{area}) / \left(\pi \times \left(\text{major axis}\right)^2\right)$$

Image Analysis—Viability from Live/Dead Staining: The percentage of the viability was calculated from the stack of images taken using ImageJ. For each channel, the maximum intensity Z-projection images were obtained using ImageJ. Then, a Gaussian blur filter was passed (sigma ball radius of 2) and the number of cells in each channel was counted using the find maxima process tool (ImageJ). The total number of cells was calculated using Equation (2) and the percentage of cell viability was calculated as per Equation (3).

Equation (2): Calculation of the total number of cells for Live/Dead staining

$$N_{\text{total}} = \text{live}_{\text{cells}} + \text{dead}_{\text{cells}}$$

where $\text{live}_{\text{cells}}$ is the total number of cells quantified using the live channel stack and $\text{dead}_{\text{cells}}$ is the total number of cells quantified using the dead channel.

Equation (3): Calculation of the viability (%) for Live/Dead staining

$$\text{Viability} \quad (\%) = \left(\text{live}_{\text{cells}}/N_{\text{total}}\right) \times 100$$

Image Analysis—YAP Localization: For YAP localization experiments, MSCs were grown in 10 mm petri dishes using growth medium. All hydrogels were polymerized and maintained in DPBS until seeding. Cells were seeded on top of the hydrogels at a density of 5000 cells cm^{-2} for 3 h in medium without serum.

The quantification of YAP was assessed from the fluorescence images using ImageJ. The nuclear/cytoplasm ratio was calculated using Equation (4).

Equation (4): YAP's integrated density fluorescence nucleus/cytoplasm ratio

$$\text{YAP}_{\text{nuc/cyt}} \text{ ratio} = \left[\left(\text{YAP}_{\text{nuc}}/A_{\text{nuc}}\right) / \left(\text{YAP}_{\text{cyt}}/A_{\text{cyt}}\right)\right]$$

where YAP_{nuc} is the integrated density of YAP in the nucleus, A_{nuc} is the area of the nucleus, YAP_{cyt} is the integrated density of YAP in the cytoplasm (Equation (5)), and A_{cyt} is the area of the cell cytoplasm (Equation (6)).

Equation (5): YAP's integrated density fluorescence in the cytoplasm

$$\text{YAP}_{\text{cyt}} = \text{YAP}_{\text{cell}} - \text{YAP}_{\text{nuc}}$$

where YAP_{cell} is the integrated density of YAP in the entire cell.

Equation (6): Definition of cytoplasmic area

$$A_{\text{cyt}} = A_{\text{cell}} - A_{\text{nuc}}$$

where A_{cell} is the area of the entire cell.

Image Analysis—Vinculin and CD44 Analysis: Vinculin images were used for FA quantification following a step-by-step method developed by Horzum et al.[63] and implementing it in ImageJ. CD44 images were analyzed using the FA analysis server using a threshold of 2 and the actin images as a cell mask.[64]

FN Release: FN was fluorescently labeled using the DyLight-488-NHS Ester kit (Thermo Fisher) following manufacturer's instructions. Briefly, FN was dialyzed against 0.5 M borate buffer (pH 8) and then mixed for 1 h at room temperature with the fluorophore. After that, the labeled protein was dialyzed again to phosphate buffer (DPBS) and kept frozen until use. Hydrogels were fabricated without FN, with FN treated with TCEP (crosslinked), or with FN without TCEP (physically trapped). Hydrogels were immersed in DPBS and kept at room temperature. DPBS was removed every day to measure fluorescence. Fluorescence was measured using a plate reader (Tecan) together with a standard curve made with the same labeled FN. Samples were fabricated in triplicate.

Statistical Analysis: The statistical analysis was performed using GraphPad Prism 6.01 software. All experiments were carried out in triplicate. All graphs represent mean ± standard deviation (SD). The goodness of fit of all datasets was assessed via D'Agostino–Pearson normality test. For comparisons of three or more groups: normally distributed populations were analyzed via analysis of variance (ANOVA) with a Tukey's post hoc test to correct for multiple comparisons; for populations not distributed normally, a Kruskal–Wallis test was used with a Dunn's post hoc test to correct for multiple comparisons. Differences among groups are stated as $p < 0.05$ (*), $p < 0.01$ (**), $p < 0.005$ (***), $p < 0.001$ (****) when differences between groups are not statistically significant (n.s.).

Supporting Information

Supporting Information is available from the Wiley Online Library or from the author.

Acknowledgements

This work was supported by EPSRC (EP/P001114/1) and a programme of research funded by the Sir Bobby Charlton Foundation. M.S.-S. acknowledges the support through a grant from the UK Regenerative Medicine Platform "Acellular/Smart Materials—3D Architecture" (MR/R015651/1). S.T. acknowledges support from the University of Glasgow through their internal scholarship funding program.

Conflict of Interest

The authors declare no conflict of interest.

Keywords

extracellular matrices, fibronectin, hyaluronic acid, mechanobiology, stem cells, hydrogel stiffness

Received: June 10, 2020
Revised: September 4, 2020
Published online: October 1, 2020

[1] A. S. Mao, J. W. Shin, D. J. Mooney, *Biomaterials* **2016**, *98*, 184.
[2] O. Chaudhuri, L. Gu, D. Klumpers, M. Darnell, S. A. Bencherif, J. C. Weaver, N. Huebsch, H. P. Lee, E. Lippens, G. N. Duda, D. J. Mooney, *Nat. Mater.* **2016**, *15*, 326.
[3] N. Huebsch, P. R. Arany, A. S. Mao, D. Shvartsman, O. A. Ali, S. A. Bencherif, J. Rivera-Feliciano, D. J. Mooney, *Nat. Mater.* **2010**, *9*, 518.
[4] S. R. Caliari, S. L. Vega, M. Kwon, E. M. Soulas, J. A. Burdick, *Biomaterials* **2016**, *103*, 314.
[5] K. A. Kyburz, K. S. Anseth, *Ann. Biomed. Eng.* **2015**, *43*, 489.
[6] A. Shekaran, J. R. García, A. Y. Clark, T. E. Kavanaugh, A. S. Lin, R. E. Guldberg, A. J. García, *Biomaterials* **2014**, *35*, 5453.
[7] A. J. Engler, S. Sen, H. L. Sweeney, D. E. Discher, *Cell* **2006**, *126*, 677.
[8] G. Kogan, L. Šoltés, R. Stern, P. Gemeiner, *Biotechnol. Lett.* **2007**, *29*, 17.
[9] W. Y. J. Chen, G. Abatangelo, *Wound Repair Regener.* **1999**, *7*, 79.
[10] C. B. Highley, G. D. Prestwich, J. A. Burdick, *Curr. Opin. Biotechnol.* **2016**, *40*, 35.
[11] B. P. Toole, *Nat. Rev. Cancer* **2004**, *4*, 528.
[12] S. Amorim, C. A. Reis, R. L. Reis, R. A. Pires, *Trends Biotechnol.* **2020**, *6*, 1.
[13] H. Zhu, N. Mitsuhashi, A. Klein, L. W. Barsky, K. Weinberg, M. L. Barr, A. Demetriou, G. D. Wu, *Stem Cells* **2006**, *24*, 928.
[14] X. H. Bian, G. Y. Zhou, L. N. Wang, J. F. Ma, Q. L. Fan, N. Liu, Y. Bai, W. Guo, Y. Q. Wang, G. P. Sun, P. He, X. Yang, X. S. Su, F. Du, G. F. Zhao, J. N. Miao, L. Ma, L. Q. Zheng, D. T. Li, J. M. Feng, *Kidney Blood Pressure Res.* **2014**, *38*, 11.
[15] B. P. Purcell, J. A. Elser, A. Mu, K. B. Margulies, J. A. Burdick, *Biomaterials* **2012**, *33*, 7849.
[16] S. Gerecht, J. A. Burdick, L. S. Ferreira, S. A. Townsend, R. Langer, G. Vunjak-Novakovic, *Proc. Natl. Acad. Sci. USA* **2007**, *104*, 11298.
[17] M. Y. Kwon, S. L. Vega, W. M. Gramlich, M. Kim, R. L. Mauck, J. A. Burdick, *Adv. Healthcare Mater.* **2018**, *7*, 1701199.
[18] Q. Feng, M. Zhu, K. Wei, L. Bian, *PLoS One* **2014**, *9*, e99587.
[19] C. B. Highley, G. D. Prestwich, J. A. Burdick, *Curr. Opin. Biotechnol.* **2016**, *40*, 35.
[20] Y. Cai, E. López-Ruiz, J. Wengel, L. B. Creemers, K. A. Howard, *J. Controlled Release* **2017**, *253*, 153.
[21] J. Y. Lai, *Carbohydr. Polym.* **2014**, *101*, 203.
[22] W. M. Gramlich, I. L. Kim, J. A. Burdick, *Biomaterials* **2013**, *34*, 9803.
[23] C. E. Hoyle, C. N. Bowman, *Angew. Chem., Int. Ed.* **2010**, *49*, 1540.
[24] B. D. Fairbanks, M. P. Schwartz, A. E. Halevi, C. R. Nuttelman, C. N. Bowman, K. S. Anseth, *Adv. Mater.* **2009**, *21*, 5005.
[25] J. D. McCall, K. S. Anseth, *Biomacromolecules* **2012**, *13*, 2410.
[26] C. N. Salinas, K. S. Anseth, *J. Tissue Eng. Regener. Med.* **2008**, *2*, 296.
[27] U. Hersel, C. Dahmen, H. Kessler, *Biomaterials* **2003**, *24*, 4385.
[28] T. A. Petrie, J. R. Capadona, C. D. Reyes, A. J. García, *Biomaterials* **2006**, *27*, 5459.
[29] G. Altankov, F. Grinnell, T. Groth, *J. Biomed. Mater. Res.* **1996**, *30*, 385.
[30] D. J. Donaldson, J. T. Mahan, *J. Cell Sci.* **1983**, *62*, 117.
[31] A. Elosegui-Artola, R. Oria, Y. Chen, A. Kosmalska, C. Pérez-González, N. Castro, C. Zhu, X. Trepat, P. Roca-Cusachs, *Nat. Cell Biol.* **2016**, *18*, 540.
[32] D. Missirlis, J. P. Spatz, *Biomacromolecules* **2014**, *15*, 195.
[33] L. Baugh, V. Vogel, *J. Biomed. Mater. Res., Part A* **2004**, *69*, 525.
[34] M. Bieniek, V. Llopis-Hernandez, K. Douglas, M. Salmeron-Sanchez, C. Lorenz, *Adv. Theory Simul.* **2019**, *2*, 1900169.
[35] M. M. Martino, J. A. Hubbell, *FASEB J.* **2010**, *24*, 4711.
[36] M. M. Martino, F. Tortelli, M. Mochizuki, S. Traub, D. Ben-David, G. A. Kuhn, R. Müller, E. Livne, S. A. Eming, J. A. Hubbell, *Sci. Transl. Med.* **2011**, *3*, 100.
[37] V. Llopis-Hernández, M. Cantini, C. González-García, Z. A. Cheng, J. Yang, P. M. Tsimbouri, A. J. García, M. J. Dalby, M. Salmerón-Sánchez, *Sci. Adv.* **2016**, *2*, e1600188.
[38] V. Moulisová, C. Gonzalez-García, M. Cantini, A. Rodrigo-Navarro, J. Weaver, M. Costell, R. Sabater i Serra, M. J. Dalby, A. J. García, M. Salmerón-Sánchez, *Biomaterials* **2017**, *126*, 61.
[39] M. Leiss, K. Beckmann, A. Girós, M. Costell, R. Fässler, *Curr. Opin. Cell Biol.* **2008**, *20*, 502.
[40] J. E. Schwarzbauer, *J. Cell Biol.* **1991**, *113*, 1463.
[41] R. Pankov, *J. Cell Sci.* **2002**, *115*, 3861.
[42] A. Woods, R. L. Longley, S. Tumova, J. R. Couchman, *Arch. Biochem. Biophys.* **2000**, *374*, 66.
[43] E. A. Wayner, A. Garcia-Pardo, M. J. Humphries, J. A. McDonald, W. G. Carter, *J. Cell Biol.* **1989**, *109*, 1321.
[44] S. Trujillo, C. Gonzalez-Garcia, P. Rico, A. Reid, J. Windmill, M. J. Dalby, M. Salmeron-Sanchez, *Biomaterials* **2020**, *252*, 120104.
[45] L. Almany, D. Seliktar, *Biomaterials* **2005**, *26*, 2467.
[46] L. Ren, J. Zhang, X. Bai, C. G. Hardy, K. D. Shimizu, C. Tang, *Chem. Sci.* **2012**, *3*, 580.
[47] A. Chopra, M. E. Murray, F. J. Byfield, M. G. Mendez, R. Halleluyan, D. J. Restle, D. Raz-Ben Aroush, P. A. Galie, K. Pogoda, R. Bucki, C. Marcinkiewicz, G. D. Prestwich, T. I. Zarembinski, C. S. Chen, E. Puré, J. Y. Kresh, P. A. Janmey, *Biomaterials* **2014**, *35*, 71.
[48] S. Khetan, M. Guvendiren, W. R. Legant, D. M. Cohen, C. S. Chen, J. A. Burdick, *Nat. Mater.* **2013**, *12*, 458.
[49] S. K. Seidlits, C. T. Drinnan, R. R. Petersen, J. B. Shear, L. J. Suggs, C. E. Schmidt, *Acta Biomater.* **2011**, *7*, 2401.
[50] S. L. Vega, M. Y. Kwon, K. H. Song, C. Wang, R. L. Mauck, L. Han, J. A. Burdick, *Nat. Commun.* **2018**, *9*, 614.
[51] A. Lueckgen, D. S. Garske, A. Ellinghaus, D. J. Mooney, G. N. Duda, A. Cipitria, *Biomaterials* **2019**, *217*, 119294.
[52] A. Lueckgen, D. S. Garske, A. Ellinghaus, R. M. Desai, A. G. Stafford, D. J. Mooney, G. N. Duda, A. Cipitria, *Biomaterials* **2018**, *181*, 189.
[53] L. Bian, M. Guvendiren, R. L. Mauck, J. A. Burdick, *Proc. Natl. Acad. Sci. USA* **2013**, *110*, 10117.
[54] M. Y. Kwon, C. Wang, J. H. Galarraga, E. Puré, L. Han, J. A. Burdick, *Biomaterials* **2019**, *222*, 119451.
[55] S. Dupont, L. Morsut, M. Aragona, E. Enzo, S. Giulitti, M. Cordenonsi, F. Zanconato, J. Le Digabel, M. Forcato, S. Bicciato, N. Elvassore, S. Piccolo, *Nature* **2011**, *474*, 179.
[56] A. Elosegui-Artola, E. Bazellières, M. D. Allen, I. Andreu, R. Oria, R. Sunyer, J. J. Gomm, J. F. Marshall, J. L. Jones, X. Trepat, P. Roca-Cusachs, *Nat. Mater.* **2014**, *13*, 631.
[57] R. Oria, T. Wiegand, J. Escribano, A. Elosegui-Artola, J. J. Uriarte, C. Moreno-Pulido, I. Platzman, P. Delcanale, L. Albertazzi, D. Navajas, X. Trepat, J. M. García-Aznar, E. A. Cavalcanti-Adam, P. Roca-Cusachs, *Nature* **2017**, *7*, 53.
[58] M. Kantlehner, P. Schaffner, D. Finsinger, J. Meyer, A. Jonczyk, B. Diefenbach, B. Nies, G. Hölzemann, S. L. Goodman, H. Kessler, *ChemBioChem* **2000**, *1*, 107.
[59] S. P. Massia, J. A. Hubbell, *J. Cell Biol.* **1991**, *114*, 1089.
[60] J. A. Rowley, D. J. Mooney, *J. Biomed. Mater. Res.* **2002**, *60*, 217.
[61] B. D. Fairbanks, M. P. Schwartz, A. E. Halevi, C. R. Nuttelman, C. N. Bowman, K. S. Anseth, *Adv. Mater.* **2009**, *21*, 5005.
[62] B. D. Cosgrove, K. L. Mui, T. P. Driscoll, S. R. Caliari, K. D. Mehta, R. K. Assoian, J. A. Burdick, R. L. Mauck, *Nat. Mater.* **2016**, *15*, 1297.
[63] U. Horzum, B. Ozdil, D. Pesen-Okvur, *MethodsX* **2014**, *1*, 56.
[64] M. E. Berginski, S. M. Gomez, *F1000Research* **2013**, *2*, 68.

